Bioenzymatic detection of troponin C using micro-opto-electro-mechanical systems

Jeetender Amritsar
Ion Stiharu
Muthukumaran Packirisamy
Concordia University
Micromechatronics Laboratory
Concave Research Center
1455 de Maisonneuve Boulevard
Montreal, Quebec H3G 1M8 Canada
E-mail: js_amrit@alcor.concordia.ca

Abstract. Diagnosis and monitoring of critical diseases such as acute myocardial infarction (AMI) require a quantitative analysis of biological molecules. A high-throughput identification of these biological molecules can be generated by using micro-electro-mechanical systems (MEMS) structures like simple cantilever beams, which respond to the intermolecular forces resulting from binding these molecules. Biochemical markers like troponin C are considered the primary markers for myocardial injury and have generated considerable interest. A 26-residue lytic membrane protein of bee venom melittin (ME) is chosen to interact with rabbit skeletal muscle troponin C (TnC) on the surface of the cantilever beams. An optical beam deflection method is employed to identify the enzymatic reaction on the surface of the cantilever due to these proteins. Identification of these proteins is also done using fluorescence spectroscopy (FS) to compliment the optical monitored deflection method. A second set of proteins like horse raddish peroxide (HRP) and hydrogen peroxide (H_2O_2) are applied to atomic force microscopy (AFM) cantilever beams to study their behavior under the enzymatic reactions of proteins. Identification of these proteins is done using Fourier transform infrared spectroscopy (FTIR). An analytical model of the cantilever beam is developed, and its mode shapes are studied by employing orthogonal polynomials in the classic Rayleigh-Ritz method. The surface stress caused by the enzymatic reaction of the proteins that leads to pure bending on the top surface of the cantilever is evaluated. The information provided by the experimental and analytical modeling reported in this work will be useful in the development of a portable biosensor for the detection of AMI. © *2006 Society of Photo-Optical Instrumentation Engineers.* [DOI: 10.1117/1.2186326]

1 Introduction

Diagnosis of acute myocardial infarction (AMI) has received much attention in recent years.[1] Although it is still difficult to evaluate myocardial damage in the early phase of its occurrence, an effort has been made to detect the enzymes that run early into the blood after the infarction.[2] Creatine kinase and troponins have been reported to be very cardiac specific and also correlate well with the severity of the myocardial damage. However, they appear very slowly in the blood stream and need plenty of time to reach their peak.[3] In spite of this, the measurement of troponins in the assessment of cardiac damage and diseases is now widespread throughout due to their longer lead times.[4] For patients with severe chest pain, this troponin can provide risk stratification for the long term.[5] But these tests are usually done in hospitals at a huge cost.

Point-of-care testing provides a reasonable solution to the costs associated to the hospitalization of false-negative cases.

A great deal of scientific research has been devoted to develop biosensors incorporated with microdevices that could provide instant results. Biosensors that have mainly focused on the analysis of proteins and enzymes have attracted considerable attention.[6] These microdevices have been termed as "ideal"[6] structures for analyzing and sensing these enzymes due to the reduced geometry that requires minute quantity of analytes. Microfabricated cantilevers have been proposed as preferable structures for biosensing applications.[7] By applying mass on the cantilever, a change in its resonant frequency and surface stress can be monitored easily,[8,9] since the mass of troponin added in the present study is in mg per ml compared to its quantity of ng per ml in blood. Previous work[10] has been done on microarrays of cantilevers to detect multiple unlabelled biomolecules at minute concentrations. The deflection of this mass-loaded cantilever beam can be evaluated with

Address all correspondence to Jeetender Amritsar , Concordia University, Micromechatronics Laboratory, 1455 de Maisonneuve Boulevard, Montreal, Quebec H3G 1M8 Canada. Tel: 514–581–5338; Fax: 514–848–8635; E-mail: js_amrit@alcor.concordia.ca
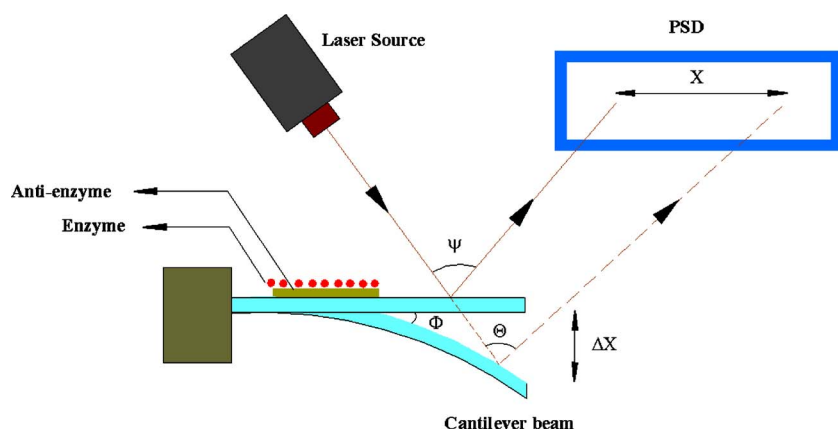
Fig. 1 Schematic of optical beam deflection system.

many optical detection techniques. Biomolecular interaction between target and probe molecules produces a sufficiently large force, which produces a surface stress, to bend the cantilever beam and produce motion that was detected optically.[11] DNA hybridization and receptor ligand binding produces a surface stress on the cantilever that causes it bend.[12] The differential deflection of the cantilevers was found to provide a true molecular recognition signal despite large nonspecific responses of individual cantilevers.

Any measurable disturbances in the normal behavior of a microcantilever beam are of interest in the detection of enzymes-antienzymes reaction patterns. Thus, deflection, natural frequency, or vibration modes of the cantilever beam are determined by the Rayleigh-Ritz method. In the present work, an effort has been made to analyze the behavior of PVDF-coated cantilever beams under the action of the enzymes optically. Similarly atomic force microscope (AFM) beams made of silicon were also monitored under the action of a different set of enzymes. Identification of these enzymes was also complimented by fluorescence spectroscopy (FS), and Fourier transform infrared spectroscopy (FTIR). The surface stress that is generated on the surface of the cantilevers is evaluated analytically. Scanning electron microscopy (SEM) of the enzymes on the surface was also taken.

2 Experimental Methods

2.1 Optical Beam Deflection Method Using PVDF Cantilever Beams

The experiment has been carried out in the laboratory using an optical setup. The experimental setup is presented in Fig. 1. The setup includes a low-power laser source of 1 mW and maximum wavelength of 632.8 nm to yield a beam size of around 100 to 200 μm, a spot-on complementary metal-oxide semiconductor (CMOS) camera with 3.5 million pixels, and sensitive wavelength ranging from 350 to 1100 nm. The position accuracy is less than 5 μm with a submicron resolution of less than 1 μm. It can accommodate a laser beam diameter from 100 μm to 3 mm. The overall detector size is a 4.7 $\times$3.4-mm active area. Polymer-coated aluminum beams of 2.5$\times$0.8 mm were used such that larger amounts of reactants were deposited. The reactants were deposited using an elec-

tronic pipette that can take a minimum volume of 0.2 μl to a maximum volume of 2 μl. The error percentage was less than 0.012 μl.

2.2 Identification of Enzymes Using Fourier Transform Infrared Spectrometry

A variety of analytical tools are available to study protein conformation. Of these methods, Fourier transform infrared spectrometry (FTIR) has proven to be quite versatile.[13] The versatility of FTIR is based on the long wavelengths of radiation, which minimize scattering problems. Spectral differences for proteins like troponin C (TnC) and horse radish peroxide (HRP) observed on glass samples. 22$\times$22-mm-square glass samples of 0.1 mm thickness were used to detect the spectrum. Two glass samples were used, one placed on top of the other, and a gold coating was deposited on the corners between them to provide an air gap of 1 μm to allow the proteins to bind with each other.

2.3 Fluorescence Spectral Analysis

Fluorescence spectroscopy detected TnC-bee venom melittin (ME) binding at concentrations ranging from 2, 20, and 200 μM at 1:1 complex and various other ratios. It not only determines the characteristics of single monoclonal antibodies in a short time, but also determines the characteristics of multiclonal antibodies.[13] This finding is very useful for selecting monoclonal antibodies with the best application potential. Fluorescence spectroscopy observes a very large range of radiation, which minimizes scattering problems from the irradiation source. We were able to view the spectrum ranging from 200 to 2000 nm and found the best spectral region to be 350 nm for TnC-ME binding.

3 Cantilever Model

3.1 Rayleigh-Ritz Approach

The mode shapes of the system are a complete set of orthogonal functions that are characteristics of the system. It is possible to express the deflection shape of the system in a generalized Fourier series involving mode shapes. The Rayleigh-
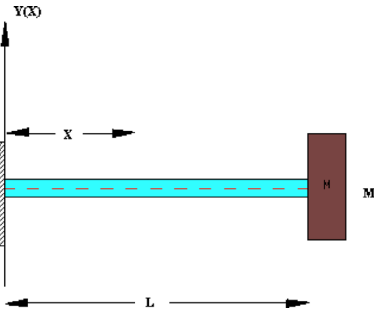
Fig. 2 Concentrated mass (M) applied at the free end of the cantilever beam of length L.

Fig. 4 Comparison of second mode shape before and after load.

Ritz method provides an approximate solution of the eigenvalue problem for a cantilever beam whose deflection function is of the linear form given by

$$W(x) = \sum_{k=1}^{n} A_k \Phi_k, \tag{1}$$

where A_k is the constant coefficients or the deflection constants, and Φ_k is the shape functions that are generated by the Gram-Schmidt process[14] and satisfy the natural boundary conditions of the beam. The expression for Rayleigh's quotient is the ratio of the maximum potential energy U_{max} to the maximum kinetic energy T^*_{max} of the system. It is given by

$$\omega^2 = \frac{U_{max}}{T^*_{max}} = \lambda, \tag{2}$$

where the kinetic energy is expressed as $T_{max} = \omega^2 T^*_{max}$ and λ is the eigenvalue. The total energy of the cantilever beam includes the potential energy, the energy due to the springs (rotational and translational), and the kinetic energies.[15] Hence the maximum potential energy of the system becomes $U_{max} = U_b + U_s$. Here, U_b is the strain energy of the cantilever and is given by

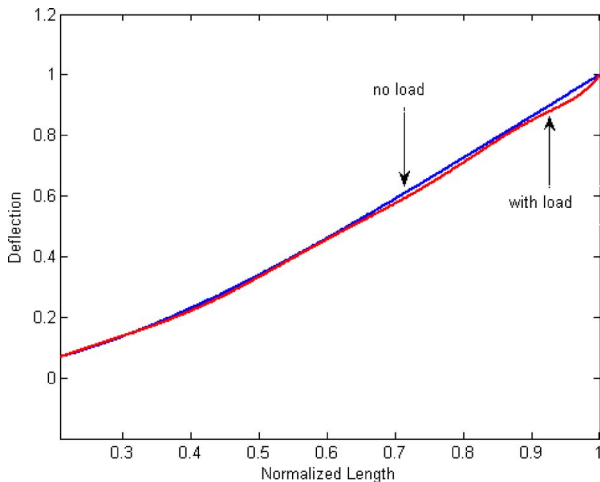$$U_b = \frac{EI}{2L3} \int_0^L [W''(x)]^2 dx. \tag{3}$$

U_s is the maximum potential energy due to the springs and is given by

$$U_s = \frac{1}{2} K_T [W(0)]^2 + \frac{1}{2} \frac{K_R}{L^2} [W'(0)]^2. \tag{4}$$

T_b is the maximum kinetic energy of the beam and is given by

$$T_b = \frac{1}{2} \rho A L \omega^2 \int_0^L [W(x)]^2 dx, \tag{5}$$

where ρ, A, and L are the material density, cross sectional area, and the length of the beam, respectively, and ω is the natural frequency in radiance per second. Substituting the deflection function of Eq. (1) into the kinetic and potential energies in Eqs. (3)–(5), the Rayleigh quotient in Eq. (2) is
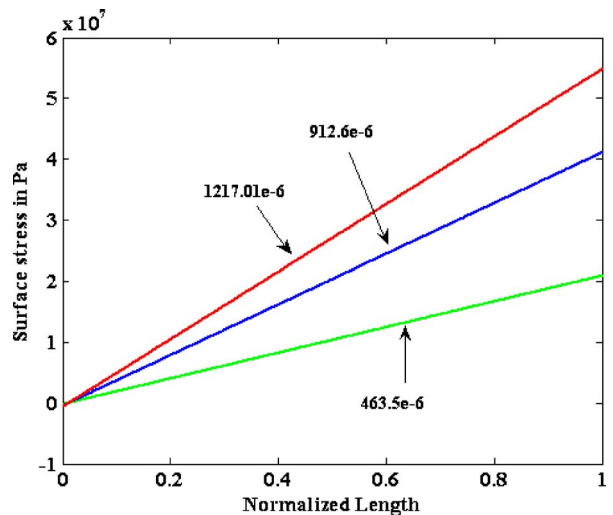

Fig. 3 Comparison of first mode shape before and after load.

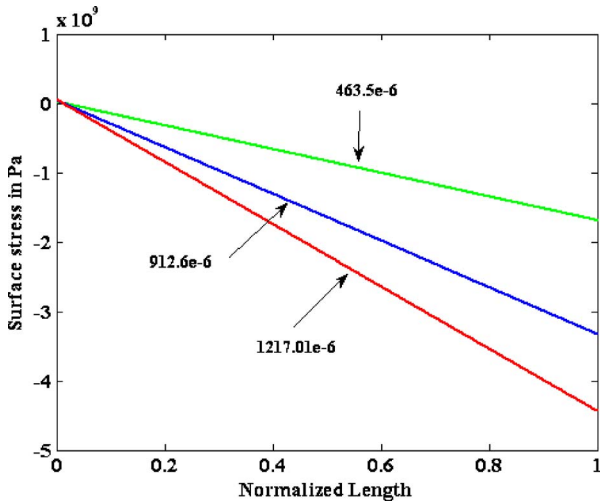**Fig. 5** Tensile surface stress distribution for different deflections in a PVDF beam.

Fig. 6 Compressive surface stress distribution for different deflections in an AFM beam.

given in terms of the coefficients A_k, which minimizes into the eigenvalue equation that is given in the form

$$\sum_n [C_{n,i} + C_{n,i}^S - \lambda^2 E_{n,i}^{0,0}]A_n = 0, \qquad (6)$$

where

$$C_{n,i} = \int_0^L \left[\frac{d^2\Phi_n(x)}{dx^2} \right]\left[\frac{d^2\Phi_i(x)}{dx^2} \right]dx,$$

$$C_{n,i}^S = K_T^* \Phi_n(0)\Phi_i(0) + K_R^* \Phi_n'(0)\Phi_i'(0),$$

$$E_{n,i}^{0,0} = \int_0^L \Phi_n(x)\Phi_i(x)dx,$$

$$K_T^* = \frac{K_T L^3}{EI}, \quad K_R^* = \frac{K_R L}{EI}, \quad \lambda^2 = \frac{\rho A \omega^2 L^4}{EI}. \qquad (7)$$

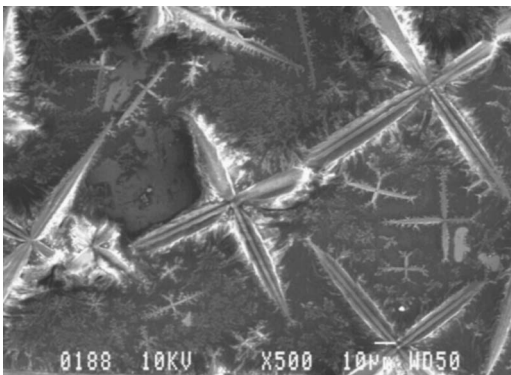The natural frequency of the cantilever beam then relates to the expression given as

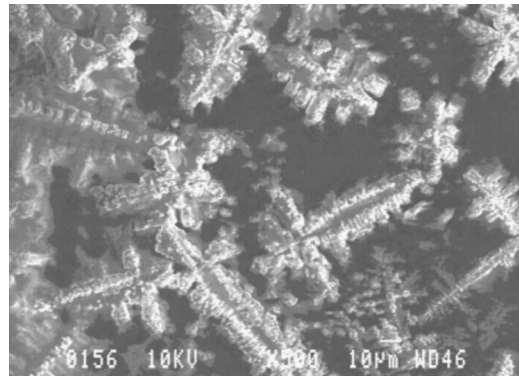**Fig. 7** TnC-ME binding at 40 mg/ml.

Fig. 8 TnC-ME binding at 20 mg/ml.

$$\omega_n = \lambda_n \left(\frac{EI}{\rho A L^4} \right)^{\frac{1}{2}}, \qquad (8)$$

where the λ_n are the eigenvalues, E is the Young's modulus of elasticity, and I is the moment of inertia of the beam.

3.2 Application of Load

This droplet can be assumed to be a concentrated mass applied at the free end of the cantilever beam for simplicity in modeling, as shown in Fig. 2. The kinetic energy of the system becomes

$$T_b = \frac{1}{2}\rho A L \omega^2 \int_0^L [W(x)]^2 dx + \frac{1}{2}M[W(L)]^2 dx. \qquad (9)$$

Equation (9) can be written as follows:

$$T_b = \frac{1}{2}\int_0^L \sum_n \Phi_n(x)\Phi_i(x)dx + \frac{1}{2}\sum_n M\Phi_n(L)\Phi_i(L). \quad (10)$$

Equation (10) gives an expression for the evaluation of concentrated mass at the free end of the cantilever beam. Due to the addition of this extra mass, a variation in the first- and second-mode shapes can be seen in Figs. 3 and 4.

The modal analysis approach reduces the analysis time and effort, and provides results that are good engineering approximations to the actual results.
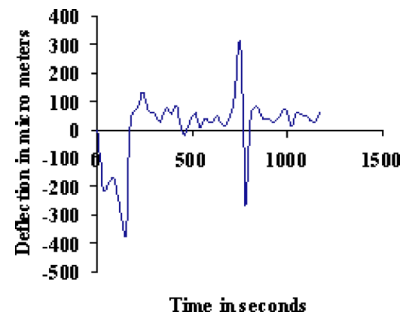

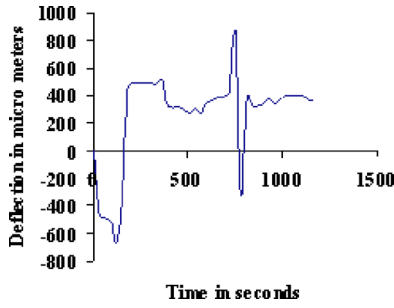**Fig. 9** PSD reading of cantilever deflection for 20-mg/ml TnC-ME at 0.4 μl.

Fig. 10 PSD reading of cantilever deflection for 40-mg/ml TnC-ME at 0.4 μl.

3.3 Evaluation of Surface Stress

When a cantilever beam is deformed in pure bending, we expect a uniaxial stress that is applied at three different points of the beam: at $y=0$; the bottom surface of the beam, which is compressive; at $y=h/2$; the middle section of the beam: and $y=h$, the top surface of the beam, which is tensile. All the other stress components are identically zero.[16] Shanley[17] demonstrated a dependency relating surface stress σ_{xx} with the cantilever tip deflection δ along the x direction based on a few assumptions. The variation of σ_{xx} is given by

$$\sigma_{xx}(x,y) = \frac{3E\delta}{2L^3}(L-x)\left[-1+\frac{2y}{h}\right], \qquad (11)$$

where δ is the deflection of the cantilever beam at a distance x, E is the Young's modulus of elasticity, L is the length of the beam, and h is the thickness of the beam.

The tensile stress on the top surface of the cantilever beam in Fig. 5 reaches to 55 MPa for a deflection of 1217.01 μm. The stress variation decreases as the deflection decreases. But in the case of the bottom surface of the beam, the surface stress goes to about −4.5 MPa (see Fig. 6). The increase in this large value of stress is unclear at present. Experimental measurements of these structures need to be in accordance with the analytical and numerical modeling for characterizing the local stresses developed.
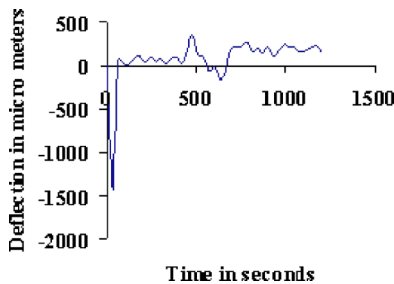

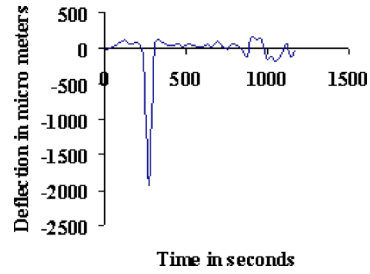**Fig. 11** PSD reading of cantilever deflection for 20-mg/ml TnC-water at 0.4 μl.

Fig. 12 PSD reading of cantilever deflection for 40-mg/ml TnC-water at 0.4 μl.

4 Experimental Results and Discussion

4.1 Measurement of Deformation Using Biochemical Reaction

Earlier experiments were carried out using optical detection techniques on AFM cantilevers on a different set of enzymes.[18] The present work strongly supports the previous results with more confidence. The TnC and ME proteins were mixed in 1:1 proportions at different concentrations of 20, 25, 30, 35, and 40 mg/ml and applied over the PVDF cantilever beams. During the reaction between the enzyme and the anti-enzyme, the chains of enzyme molecules are opening and stretching, such that it makes the cantilever beam deflect.[18] This deflection is recorded using the PSD. Once the buffer solution evaporates, the remaining solid phase on the beam arranges it self in a texture-like configuration, such that it will create a permanent stress and a strain in the cantilever. To support these assumption, SEMs of TnC-ME are shown in Figs. 7 and 8. The binding of TnC-ME is shown in the SEM picture after complete evaporation of the buffered solution.

Bee venom melittin (26-residue membrane obtained from the venom of honey bees) binds to skeletal muscle troponin C (molecular weight of 18,000 Daltons and is 70 Å long) with a Ca^{2+}-dependent reaction. ME is bound to troponin C irrespective of the presence or absence of Ca^{2+} in 50-mM KCl (potassium chloride) and 50-mM Tris-HCL at a pH of 7.5. Measurement of cantilever deflection was performed under the circumstances for various concentrations of TnC-ME. The pattern of measurement regardless of the concentration is always almost the same and is illustrated in Figs. 9 and 10.

The displacement in micrometers at the PSD scanner in the vertical axis is given with respect to time in seconds in the horizontal axis. The figure indicates that the loading with the organic fluid solution of the beam will create a deflection of about 10 μm, which is translated to the PSD in a negative
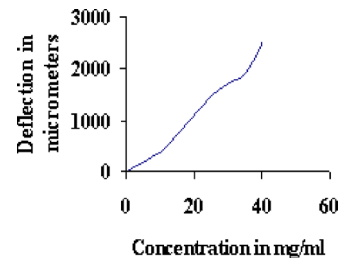

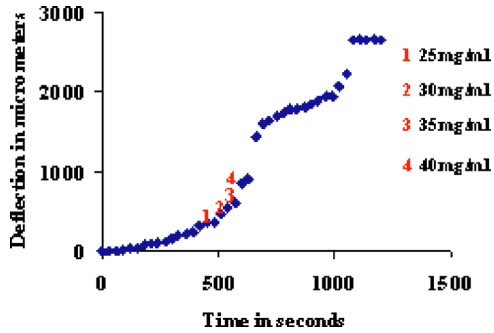**Fig. 13** Cantilever deflection as a function of TnC-ME concentration.

Fig. 14 Cantilever deflection as a function of time in seconds for TnC-ME.

Fig. 16 Fluorescence emission spectrum of TnC-ME.

(downward) displacement of the laser spot by 400 μm. Further reactions will stretch the beam more due to reorganizing of the enzyme molecules to the surface of the cantilever. The reactions count for five to six more micrometers of deflection at the cantilever, which occur in about one minute. The time duration is not quite relevant, since the volumes used in the experiments were very large. Also, the beam starts moving up by 27 μm with respect to the lowest previous occupied position. This motion is slow at a rate of about 1 μm per second. This curving up is associated with the adhesion of the enzyme molecules on the surface of the cantilevers, a phenomenon that produces a tension in the bottom surface of the beam.

This pattern of TnC-ME was compared with that of TnC-water of different concentrations. Significant differences were recorded in the pattern of displacement and amplitude. The patterns are presented in Figs. 11 and 12, respectively.

Also, troponin C binds on the surface of the cantilever, but the superficial tension produced by the troponin and water combination produces a higher deflection when compared to the troponin and melittin combination. This is relevant from the signature of reaction in Figs. 11 and 12, respectively. From the experimental setup, it was noticed that there was a time-dependent drift present in the deflection signal, and the drift in the measured signal depended almost linearly on time.[19]

As the concentration (mass) increases, the peak deflection also increases linearly, as shown in Fig. 13. The higher the concentration is, the higher the deflection. Meanwhile, at higher concentrations, the duration of the reaction is high. Also, a comparison was made between the deflection of the cantilever and the time taken. The time $t=0$ corresponds to
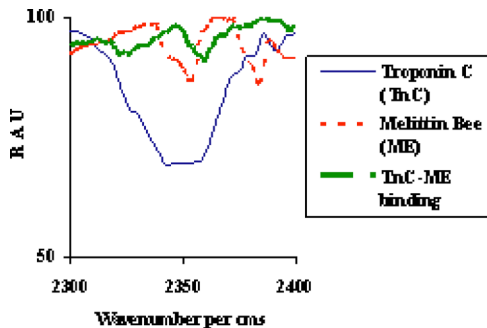
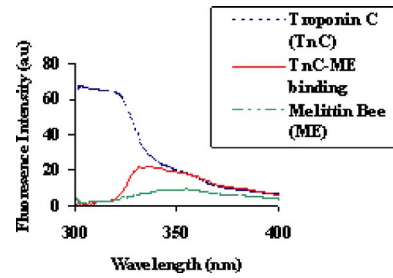the time when 0.4 μl of TnC and 0.4 μl of ME was deposited on the cantilever surface at room temperature. The PVDF cantilever exhibited a bending of $\sim$2500 μm at time $t=1100$. As seen in Fig. 14, the deflection rate becomes constant at $t=900$ when both TnC-ME evaporate completely from the surface of the cantilever. The data presented in this figure demonstrate both the high sensitivity and large dynamic range of PVDF cantilevers to TnC-ME reaction.

4.2 Spectral Analysis

Identification of the enzymatic reactions is acquired using FTIR and fluorescence spectroscopy. Both methods share the same development level. They are not available in the microsystem scale, but eventually they could all be integrated in a chip or in hybrid architecture.[20] Figures 15 and 16 indicate the comparison between ME, TnC, and TnC-ME complex due to the Ca^{2+} interaction.

Due to the presence of excess Ca^{2+}, TnC undergoes a configurational change from a dumbbell structure to a globular structure[21] when ME binds to TnC, and hence there is a change in fluorescence intensity, as in Fig. 16 near 330 nm. In the presence of excess TnC, melittin develops a significant change in the relative absorption unit (RAU), which is seen as a positive modification of the spectrum in the tryptophan (19th amino acid residue of ME) region of around 2350 per cms, as shown in Fig. 15. Also, the change in the spectrum could be due to the removal of quenching factors, such as quenching of small molecules and amino acids.

4.3 Dynamic Characteristics for Different Enzymes

The dynamic characteristics of TnC-ME were compared to that of horse raddish persoxide (HRP) and hydrogen peroxide (H_2O_2) using the FTIR. In the presence of excess TnC, ME develops a strong positive difference spectrum in the tryp-
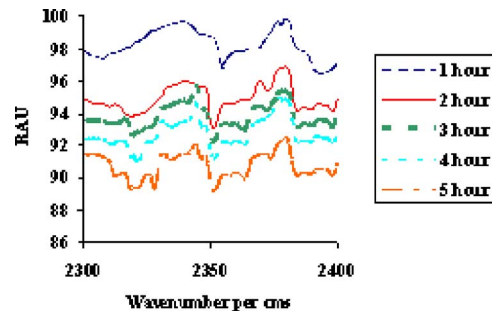

Fig. 15 TnC-ME reaction using the FTIR.

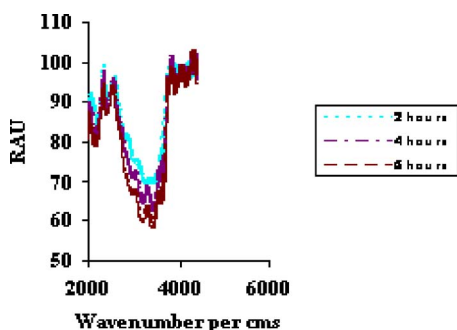**Fig. 17** Dynamic characteristics of TnC-ME for every one hour.

Fig. 18 Dynamic characteristics of HRP-H_2O_2 for every two hours.

tophan (Trp) region.[21] It remains uncertain whether the effect results from direct involvement of Trp 19 in the region of contact, or whether it arises indirectly from the altered conformation of ME. In the case of the dynamic characteristics of these two proteins, ME binding to TnC strengthens the binding of Ca^{2+} to the troponin of the complex. Thus, the TnC-ME complex is not rigidly maintained but undergoes a transition on the Ca^{2+} binding to the low-affinity Ca^{2+} binding sites. Similarly for the case of HRP-H_2O_2, the RAU increases by a good 10% every 2 h, but remains steady after a period of time, showing the stability of these two sets of proteins (see Figs. 17 and 18).

5   Conclusion

In the present study, an effort is made to study the antigen-antibody interaction between TnC-ME and compare the dynamic characteristics with that of HRP-H_2O_2. Tests are performed using the optical lever method, fluorescence spectroscopy, and FTIR to understand the variation between the proteins. The dynamic behavior of cantilever beams is analyzed under the enzymatic reaction of TnC-ME. The beams are modeled accordingly to evaluate the surface stress occurring on the upper and lower surfaces of the beam. The modal analysis is done on the cantilever beam using the Rayleigh-Ritz method to find out the system's natural frequencies and mode shapes when the system is vibrating in one of the natural frequencies.

Different optical methods used in this work give a good interpretation and understanding of the enzymatic interaction. The results summarized provide strong evidence that there is an interaction between the proteins, and this information can be used in the development of biosensors that could detect AMI.

References

1. X. Liu and J. Wei, "Determination of affinities and antigen epitopes of bovine cardiac troponin I (cTnI) with monoclonal antibodies by surface plasmon resonance biosensor," *Anal. Biochem.* **314**, 301–309 (2003).
2. K. Suzuki and Y. Sawa, "Early detection of cardiac damage with heart fatty acid-binding protein after cardiac operations," *Ann. Thorac. Surg.* **65**, 54–58 (1997).
3. V. P. Guiteras, L. C. Pelletier, M. G. Hernandez, J. M. Jais, B. R. Caitman, G. Dupres, and B. CG. Solymass, "Diagnostic criteria and prognosis of preoperative myocardial infarction following coronary bypass," *J. Thorac. Cardiovasc. Surg.* **86**, 878–886 (1983).
4. J. R. Tate, D. Heathcote, J. Rayfield, and P. E. Hickman, "The lack of standardization of cardiac troponin I assay systems," *Clin. Chim. Acta* **284**, 141–149 (1999).
5. C. W. Hamm, J. Ravkilde, W. Gerhardt, P. Jorgensen, E. Pehlim, L. Ljungdahl, B. Goldman, and H. A. Katus, "The prognostic value of serum troponin I in unstable angina," *N. Engl. J. Med.* **327**, 146–150 (1992).
6. P. V. A. Pamidi and J. Wang, "Electroanalysis and measurement of hydrazine compounds at glassy carbon electrodes coated with electropolymerized 3, 4′-dihydroxybenaldehyde films," *Electroanalysis* **8**, 244–247 (1996).
7. M. D. Antonik N. P. D'Costa, and J. H. Hoh, "A biosensor on micromechanical interrogation of living cells," *IEEE Eng. Med. Biol. Mag.* **16**, 66–72 (1997).
8. R. Berger, E. Delmarche, H. P. Lang, C. Gerber, J. K. Gimzewski, E. Meyer, and H. J. Guntherodt, "Surface stress in the self assembly of alkanethiols on gold," *Science* **276**, 2021–2023 (1997).
9. R. Raiteri, H. J. Butt, and M. Grattarola, "A sensitive method to measure changes in the surface stress of solids," *J. Colloid Interface Sci.* **180**, 251–260 (1996).
10. R. McKendry, J. Zhang, Y. Arntz, and C. Gerber, "Multiple label free biodetection and quantitative DNA-binding assays on a nanomechanical cantilever array," *Proc. Natl. Acad. Sci. U.S.A.* **99**, 9783–9788 (2002).
11. W. Guanghua, R. H. Datar, K. M. Hansen, T. Thundat, R. J. Cote, and A. Majumdar, "Bioassay of prostate-specific antigen (PSA) using micro-cantilever," *Nat. Biotechnol.* **19**, 856–860 (2001).
12. J. Fritz, M. K. Baller, H. P. Lang, H. Rothuizen, P. Vettiger, E. Meyer, H. Guntherodt, C. Gerber, and J. K. Gimzewski, "Translating biomolecular recognition into nanomechanics," *Science* **288**, 316–318 (2000).
13. P. I. Harris, "Fourier transform infrared studies of peptides: Potentials and pitfalls," *ACS Symp. Ser.* **750**, 54–95 (2000).
14. R. B. Bhat, "Natural frequencies of rectangular plates using characterization orthogonal polynomials in Rayleigh-Ritz method," *J. Sound Vib.* **102**, 493–497 (1985).
15. G. Rinaldi, M. Packirisamy, and I. G. Stiharu, "Experimental investigation on the dynamics of MEMS structures," *Proc. SPIE* **5455**, 66–73 (2004).
16. V. T. Srikar, K.. S. Anna, M. U. Selim, B. B. Goldberg, and S. M. Spearing, "Micro-Raman measurement of bending stresses in micromachined silicon flexures," *J. Microelectromech. Syst.* **12**, 779–787 (2003).
17. F. R. Shanley, *Strength of Materials*, McGraw-Hill, New York (1957).
18. J. Amritsar, I. Stiharu, and M. Packirisamy, "Micro electro mechanical systems (MEMS) for enzymatic detection," *Proc. SPIE* **5455**, 101–109 (2004).
19. P. G. Datskos and I. Sauers, "Detection of 2-mercaptoethanol using gold-coated micromachined cantilevers," *Sens. Actuators B* **B61**, 75–82 (1999).
20. J. Amritsar, I. Stiharu, and M. Packirisamy, "MOEMS for bioenzymatic detection," *Can. Inst. Photon. Innov. (CIPI)* **3**(1), 25–27 (2005).
21. J. Amritsar, I. Stiharu, and M. Packirisamy, "Enzymatic detection of troponin C and melittin bee," *Proc. SPIE* **5705**, 40–51 (2005).